# Stability and Correlation of Electrogram Organization and Synchronization Indices during Atrial Fibrillation

F Simón[1,3], A Arenal[2], P Laguna[1,3], JP Martínez[1,3]

[1]Comunications Technology Group, I3A, University of Zaragoza, Zaragoza, Spain
[2]Department of Cardiology, Gregorio Marañón General University Hospital, Madrid, Spain
[3] CIBER of Bioengineering, Biomaterials and Nanomedicine (CIBER-BBN), Spain

## Abstract

*In this work we perform a statistical study of organization and synchronization indices in electrogram (EGM) signals obtained during ablation surgery in patients with Atrial Fibrillation (AF). We have considered organization, synchronization and delay indices, obtaining by three different ways, spectral, cross-correlation and wavefront analysis: dominant frequency, $f^{\mathrm{D}}$, regularity index, $I^{\mathrm{R}}$, organization index, $I^{\mathrm{O}}$, coherence, $\Gamma$, cross-correlation, $\rho$ and $\tau$, interquartile consistency, $C^{\mathrm{IQR}}$, normalized consistency measure, $CE$, and median delay $\mu$ (computed all in 10-second excerpts). We have studied their temporal and spatial stability, and the correlation between pairs of indices. We found that all organization indices are stable measures ($\overline{CV}$<0.2) along time and a decrease in the synchronization degree with the increase of distance between electrodes.*

## 1. Introduction

Atrial fibrillation (AF) is a type of cardiac arrhythmia due to electrical re-entry in the atria. As a consequence, there is no uniform atrial contraction, inadequate blood pumping from atrium to ventricle and erratic and fast ventricular rate.

It is the most common arrhythmia (in Europe, the lifetime risk to develop AF at the age of 55 years is 23.8% in men and 22.2% in women [1]) and is a frequent cause of cardiac embolism and heart failure decompensation.

In order to reverse AF to sinus rhythm, electrical and pharmacological cardioversion are typically used. If this does not work, radio-frequency ablation is usually performed (to burn atrial zones in order to avoid electrical re-entry by means of cardiac catheterization). Different ablation methods have been proposed and are currently under investigation [2], but the main goal of ablation is to allow only one electrical way between sinoatrial and atrioventricular nodes.

During the catheterization, electrogram signals (EGM) can be obtained by locating electrodes in the cardiac walls. Analysis of EGM signals recorded at different sites provides information about local electrical activity, including regularity and synchronization between different sites. This information may be useful to determine the desirable approach to ablation.

The main goal of this work is to perform a statistical study of different organization and synchronization indices in EGM signals.

## 2. Database

We used a database recorded in Cardiac Electrophysiology Unit of the Gregorio Marañón Hospital, Madrid. It consists of 41 records from 14 patients with AF. The sampling rate is 977 Hz and the average duration is 2 minutes and 9 seconds. Bipolar EGM signals were acquired with 4 catheters: 1) Ablation Catheter (ABL, 2 leads); 2) Coronary Sinus Catheter (CS, 1 lead); 3) His Catheter (HIS, 1 lead); 4) $Lasso^{\mathrm{TM}}$ Catheter (10 leads).

In this work we focus on *lasso* leads (this 10-lead circular catheter can be located in different zones of the pulmonary veins and atrial appendages). All records of less than 40 seconds or very noisy were discarded, leaving a final dataset of 30 records.

## 3. Methods

The processing scheme for obtaining the studied indices is shown in Fig.1.

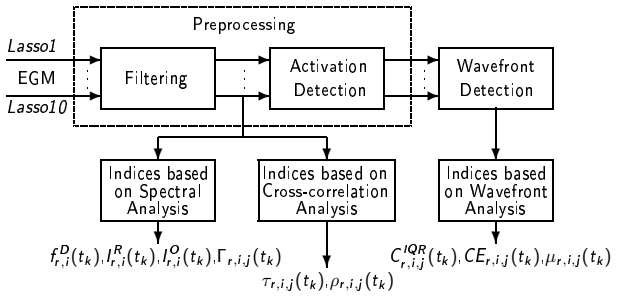


Figure 1. Block diagram of the processing steps to obtain the signal indices.

### 3.1. EGM preprocessing

**Filtering**: The following procedure based on [3] was used: after a band-pass filtering, with 40 and 250 Hz cut-off frequencies, both slow deflections and high frequency noise are attenuated. The previous signal was rectified, moving most energy to low frequencies. Finally, we applied a linear low-pass filter, with cut-off frequency of 20 Hz. Figure 2 shows the original (a) and filtered (b) EGM signals. Note that the filtered signal shows a pulse for each activation.

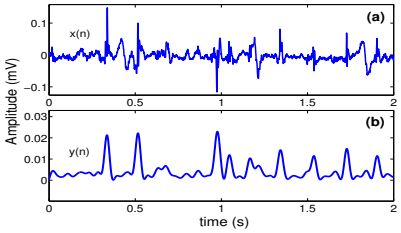


Figure 2. (a) Original EGM lead, $x(n)$. (b) Output signal after the filtering process, $y(n)$.

**Activation detection**: The detector is based on finding peaks greater than an adaptive threshold proportional to the average amplitude of the last activations [3]. In order to strengthen the activation detection process, some conditions were added to the actualization threshold rule:

- After every 200 ms without any activation detection, the threshold is reduced by 10%.
- A 50 ms safety margin or refractory period is defined after an activation detection, avoiding multiple detections.
- If the interval between two detected activations is longer than 350 ms, a new search (look-back) is performed reducing the threshold by 30%.

### 3.2. Wavefront detection

After detecting activation in each *lasso* EGM lead, we want to group those belonging to the same wavefront, as shown in Fig.3.

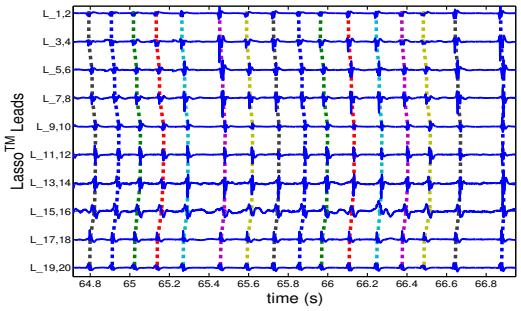


Figure 3. Activations of the *lasso* leads are grouped in wavefront (vertical lines) if they come from the same wavefront.

For this purpose we used the method proposed in [3], assuming that two activations from adjacent leads belong to the same wavefront if they are closer than 90 ms. As a result, we obtain the matrix $\boldsymbol{W} = [\, \boldsymbol{t_1}\, \boldsymbol{t_2} \ldots \boldsymbol{t_{10}} \,]^T$, whose columns contain wavefront activation instants of the studied record. The $i^{th}$ row of $\boldsymbol{W}$, $\boldsymbol{t_i}$, contains the instant activation for $i^{th}$ lead, allowing to obtain the delay vectors between the detected wavefront, $\boldsymbol{\delta}_{i,j} = \boldsymbol{t_i} - \boldsymbol{t_j}$. It should be noted that only wavefronts whose activation was detected in all leads were used.

### 3.3. Organization/Synchronization indices

**Indices based on spectral analysis**: The Welch averaged periodogram method (with 2-second windows and 50% overlap) was used to estimate the power spectral density (PSD) of each 10-s segment. As we show in Fig.4, we focus in the frequencies from 1.5 to 20 Hz ($f_{min}$ and $f_{max}$, respectively). The dominant frequency, $f^{\mathrm{D}}$, is the frequency of maximum PSD [4]. The ratio between the area under the estimation of PSD in $f^{\mathrm{D}} \pm 0,75$ Hz and the area from $f_{min}$ to $f_{max}$, was called regularity index, $I^{\mathrm{R}}$ [5]. The organization index, $I^{\mathrm{O}}$ [6], is defined in a similar way, but including the areas under the harmonic frequencies of $f^{\mathrm{D}}$ ($2 \cdot f^{\mathrm{D}} \pm 0,75$ Hz, $3 \cdot f^{\mathrm{D}} \pm 0,75$ Hz...) which are within $f_{min}$ to $f_{max}$. Both $I^{\mathrm{R}}$ and $I^{\mathrm{O}}$ tell us about how organized are the activations within an EGM lead.

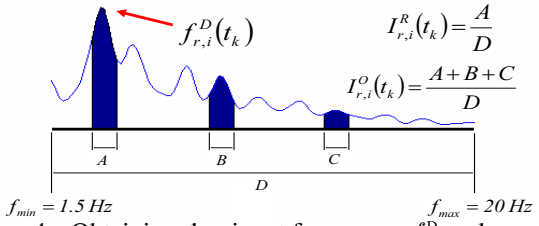


Figure 4. Obtaining dominant frequency, $f^{\mathrm{D}}$ and regularization and organization indices, $I^{\mathrm{R}}$ and $I^{\mathrm{O}}$.

In order to study the synchronization between two leads, we proposed to use the averaged coherence index, $\Gamma$, which is defined as the averaged spectral coherence modulus in $f^{\mathrm{D}}_{i,j} \pm 0,75$ Hz, where $f^{\mathrm{D}}_{i,j}$ is the dominant frequency in the cross-spectrum between $i$ and $j$ leads. $\Gamma$ will have a value near 1 if dominant periodicities of both leads are synchronized.

**Indices based on cross-correlation analysis**: The maximum normalized cross-correlation $\rho$ of each pair of leads, $y_i(n)$ and $y_j(n)$, which can be seen as a measure of synchronization, was obtained as well as the lag $\tau$ where the maximum appears.

$$\tau_{i,j} = \arg\max_{k} |r_{i,j}(k)|, \tag{1}$$

$$\rho_{i,j} = \frac{|r_{i,j}(k)|}{\sqrt{r_i(0) \cdot r_j(0)}} \ , \ with \ \ k = \tau_{i,j}, \tag{2}$$

with $r_{i,j}(k)$ the cross-correlation function between $y_i(n)$ and $y_j(n)$.

**Indices based on wavefront analysis**: A measurement of consistency of the activation delay index, $C^{\mathrm{IQR}}_{i,j}$, is obtained calculating interquartile range in $\boldsymbol{\delta}_{i,j}$ vectors. If $C^{\mathrm{IQR}}_{i,j}$ value is small, the two EGM leads are well synchronized. A normalized consistency index ($CE$), whose values go from 0 to 1 and based on the Shannon entropy of the $\boldsymbol{\delta}_{i,j}$ values [3] is also calculated.

With the wavefront detector results, we can also obtain the median delay between two leads, $\mu_{i,j}$, calculated as the median value of the delay vectors $\boldsymbol{\delta}_{i,j}$.

**In summary**: All the presented indices will take values in each 10-second window (centered in $t_k$), in each record ($r$) and for each lead ($i$) or pair of leads ($i,j$).

The described indices are of three types: 1) Inter-lead organization indices within one EGM: $f^{\mathrm{D}}_{r,i}(t_k)$, $I^{\mathrm{R}}_{r,i}(t_k)$, $I^{\mathrm{O}}_{r,i}(t_k)$; 2) Synchronization indices between two EGM: $\Gamma_{r,i,j}(t_k)$, $C^{\mathrm{IQR}}_{r,i,j}(t_k)$, $CE_{r,i,j}(t_k)$, $\rho_{r,i,j}(t_k)$; 3) Indices that determine delays between leads: $\tau_{r,i,j}(t_k)$, $\mu_{r,i,j}(t_k)$.

# 4. Results

## 4.1. EGM organization

| | | $\overline{m}\pm\overline{\sigma}$ | $\overline{CV}$ | $VR$ |
|---|---|---|---|---|
| EGM organi. | $f^{\mathrm{D}}_r$ | 6.27±0.51 (Hz) | 0.08 | 0.40 |
| | $I^{\mathrm{R}}_r$ | 0.23±0.04 | 0.19 | 0.37 |
| | $I^{\mathrm{O}}_r$ | 0.33±0.06 | 0.19 | 0.63 |
| adjacent EGM synchronization | $C^{\mathrm{IQR}}_{i,j}$ | 19.12±3.82 (ms) | 0.24 | 0.16 |
| | $CE_{i,j}$ | 0.49±0.04 | 0.09 | 0.37 |
| | $\Gamma_{i,j}$ | 0.73±0.08 | 0.14 | 0.22 |
| | $\rho_{i,j}$ | 0.79±0.04 | 0.06 | 0.27 |
| | $\lvert\tau_{i,j}\rvert$ | 7.84±5.86 (ms) | 0.79 | 1.40 |
| | $\lvert\mu_{i,j}\rvert$ | 4.31±2.14 (ms) | 0.69 | 0.40 |
| antipodal EGM synchronization | $C^{\mathrm{IQR}}_{i,j}$ | 35.59±7.03 (ms) | 0.23 | 0.28 |
| | $CE_{i,j}$ | 0.33±0.04 | 0.14 | 0.08 |
| | $\Gamma_{i,j}$ | 0.55±0.11 | 0.22 | 0.31 |
| | $\rho_{i,j}$ | 0.68±0.05 | 0.08 | 0.25 |
| | $\lvert\tau_{i,j}\rvert$ | 23.86±14.67 (ms) | 0.68 | 1.80 |
| | $\lvert\mu_{i,j}\rvert$ | 9.53±4.45 (ms) | 0.70 | 0.35 |

Table 1. Values for $\overline{m}\pm\overline{\sigma}$, $\overline{CV}$ and $VR$ are presented for all the organization and synchronization indices (for adjacent and antipodal pairs of leads).

Table 1 (first three rows) shows the mean of each lead average ($\overline{m}$), the mean of the standard deviations in each lead ($\overline{\sigma}$), the coefficient of variation ($\overline{CV}$) and variance ratio (VR) defined as the ratio between intra-lead and inter-lead variances ($VR$), for $f^{\mathrm{D}}$, $I^{\mathrm{R}}$ and $I^{\mathrm{O}}$ indices, in order to study the measure stability over time. In Figure 5 we show a scatter plot of the mean values of $I^{\mathrm{R}}$ versus $\sigma_{f^{\mathrm{D}}}$ (up) and $I^{\mathrm{O}}$ versus $\sigma_{f^{\mathrm{D}}}$ (down) in each lead, where $\sigma_{f^{\mathrm{D}}}$ is the standard deviation of $f^{\mathrm{D}}$.

## 4.2. EGM synchronization

Again, $\overline{m}$, $\overline{\sigma}$, $\overline{CV}$ and $VR$ are calculated for $C^{\mathrm{IQR}}_{i,j}$, $CE$, $\Gamma_{i,j}$ and $\rho_{i,j}$ indices.

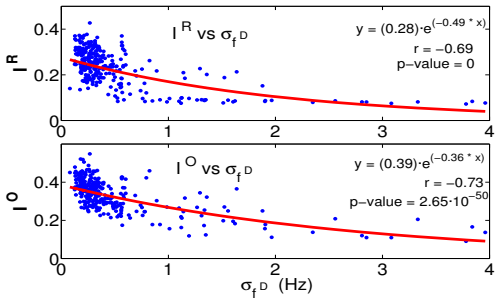


Figure 5. $I^{\mathrm{R}}$ (up) and $I^{\mathrm{O}}$ (down) versus $\sigma_{f^{\mathrm{D}}}$. Leads with unstable $f^{\mathrm{D}}$ present lower values of $I^{\mathrm{R}}$ and $I^{\mathrm{O}}$.

To simplify the analysis, we show the results for pairs of leads with separation $\pm1$ (adjacent leads) and $\pm5$ (antipodal leads).

Table 2 shows the linear correlation coefficients between the four synchronization indices studied, for adjacent (above the diagonal) and antipodal (below the diagonal) leads.

| | $C^{\mathrm{IQR}}_{i,j}$ | $CE$ | $\Gamma_{i,j}$ | $\rho_{i,j}$ |
|---|---|---|---|---|
| $C^{\mathrm{IQR}}_{i,j}$ | - | -0.87 | -0.83 | -0.34 |
| $CE$ | -0.90 | - | 0.70 | 0.54 |
| $\Gamma_{i,j}$ | -0.79 | 0.75 | - | 0.21 |
| $\rho_{i,j}$ | -0.40 | 0.55 | 0.26 | - |

Table 2. Linear correlation coefficients between the synchronization indices in the EGM adjacent (above the diagonal) and antipodal (below) leads.

Figure 6 shows the values of the synchronization indices $C^{\mathrm{IQR}}$ and $CE$ in all the database leads.

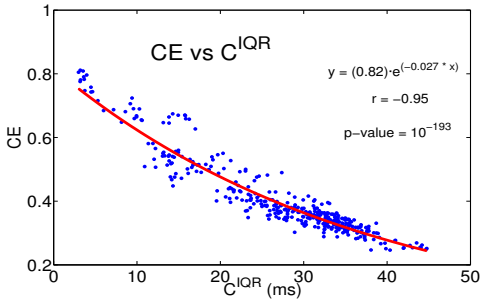


Figure 6. Relationship between the interquartile range index, $C^{\mathrm{IQR}}$ and the normalized consistency index, $CE$. Values are averaged in each lead.

Also synchronization indices based on the distance between leads have been studied. In figure 7, the mean values of the synchronization indices versus separation between leads are shown.

## 4.3. Lead delays

In this section, we compare the two methods used to determine inter-lead delays, lag where the maximum of the cross-correlation appears ($\tau_{i,j}$) and the median delay

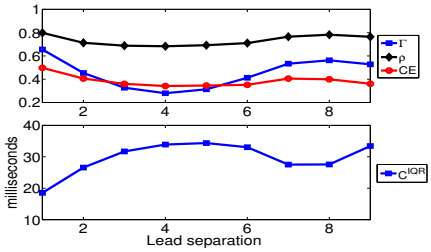


Figure 7. Average values of synchronization and delay indices versus separation between leads.

($\mu_{i,j}$). These two indices present a linear coefficient correlation of 0.71 ($p = 10^{-208}$), with no differences between adjacent and antipodal leads. Figure 8 shows a Bland-Altman diagram between $\tau_{i,j}$ and $\mu_{i,j}$.

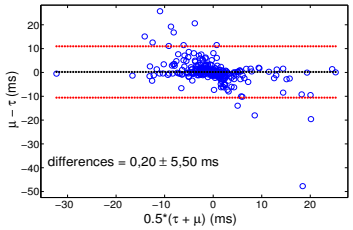


Figure 8. Bland-Altman plot between the two indices that determine delays between leads, $\tau_{i,j}$ and $\mu_{i,j}$. Horizontal lines show the mean value and $\pm$ 1.96 times the standard deviation.

## 5. Discussion and conclusions

We can conclude that, in a stationary situation, organization indices based on spectral analysis ($f_r^{\mathrm{D}}$, $I_r^{\mathrm{R}}$ and $I_r^{\mathrm{O}}$) are stable measures ($\overline{CV}$<0.2) which characterize the activity in the studied cardiac area (table 1).

Figure 5 shows a significant negative correlation (exponential regression) between the intra-lead standard deviation of $f^{\mathrm{D}}$ ($\sigma_{f^{\mathrm{D}}}$) and the organization indices $I^{\mathrm{R}}$ and $I^{\mathrm{O}}$ (observed no linear correlation between $f^{\mathrm{D}}$ and the organization indices). So leads with unstable $f^{\mathrm{D}}$ present lower values of $I^{\mathrm{R}}$ and $I^{\mathrm{O}}$ than those with a stable $f^{\mathrm{D}}$.

A moderate temporal stability has been observed in synchronization indices ($C_{i,j}^{\mathrm{IQR}}$, $CE$, $\Gamma_{i,j}$ and $\rho_{i,j}$; see table 1) between each pair of leads, both adjacent and antipodal, noting a great stability in the consistency index of the activation delay, $CE$, and the maximum normalized cross-correlation index, $\rho$ ($\overline{CV} < 0.15$).

On the other hand, looking at values in Table 2, we can affirm that a high linear correlation exists between $C_{i,j}^{\mathrm{IQR}}$, $CE$ and $\Gamma_{i,j}$ indices, both adjacent and antipodal leads, although they are indices calculated by different methods ($|r| \geq 0.70$ in all cases). A lower correlation was observed between $\rho_{i,j}$ and the other synchronization indices ($|r| \leq 0.55$). The scatter diagram of $C_{i,j}^{\mathrm{IQR}}$ and $CE$ (Fig. 6) shows a high non-linear correlation between them (exponential regression, $r = -0.95$).

As expected, a decrease in the synchronization and consistency indices with the increase of the separation between *lasso* electrodes is also shown (decrease of $\Gamma$, $\rho$ y $CE$, increase of $C^{\mathrm{IQR}}$) (see Fig. 7): re-calling the circular shape of the *lasso* catheter, synchronization is reduced when the separation increases (separation 1 to 5) and synchronization grows back for separation 5 to 9. With separation 8 and 9 the original values are not reached due to a greater or lesser degree of closure of the circular *lasso* catheter. It should be noted that $\rho_{i,j}$ index shows badly the synchronization loss and together with the lower correlation with the other indices, this suggests that is the less desirable for the synchronization analysis.

As for the delay indices, $\tau_{i,j}$ and $\mu_{i,j}$, a high correlation between them was found, obtaining concordant values in most cases (Fig. 8; 0.20 $\pm$ 5.50 ms as mean value $\pm$ standard deviation for the differences).

## Acknowledgements

Study supported by Project TEC 2007-68076-C02-02 from CICYT and FEDER, Diputación General de Aragón (DGA), Spain, through Grupos Consolidados GTC ref:T30 and CIBER-BBN (CIBER of Bioengineering, Biomaterials and Nanomedicine is an initiative of ISCIII).

## References

[1] Heeringa J, van der Kuip DA, Hofman A, Kors JA, van Herpen G, Stricker BH, Stijnen T, Lip GY, Witteman JC. Prevalence, incidence and lifetime risk of atrial fibrillation: the rotterdam study. European heart journal 2006;27(8):949–953.

[2] Cappato R, Calkins H, Chen SA, Davies W, Iesaka Y, Kalman J, Kim YH, Klein G, Packer D, Skanes A. Worldwide survey on the methods, efficacy, and safety of catheter ablation for human atrial fibrillation. Circulation 2005; 111(9):1100–1105.

[3] Richter U, Stridh M, Husser D, Cannom DS, Bhandari AK, Bollmann A, L.Sörnmo. Wavefront detection from intra-atrial recordings. Computers in Cardiology 2007;97–100.

[4] Ng J, Kadish AH, Goldberger JJ. Effect of electrogram characteristics on the relationship of dominant frequency to atrial activation rate in atrial fibrillation. Heart rhythm the official journal of the Heart Rhythm Society 2006;3(11):1295–1305.

[5] Fischer G, Stuhlinger MC, Nowak CN, Wieser L, Tilg B, Hintringer F. On computing dominant frequency from bipolar intracardiac electrograms. IEEE Transactions on Bio medical Engineering 2007;54(1):165–169.

[6] Everett TH, Kok LC, Vaughn RH, Moorman JR, Haines DE. Frequency domain algorithm for quantifying atrial fibrillation organization to increase defibrillation efficacy. IEEE Transactions on Bio medical Engineering 2001;48:969–78.

Address for correspondence:
Fernando Simón Vadillo
fsimon@unizar.es